A haploid genetic screen identifies the major facilitator domain containing 2A (MFSD2A) transporter as a key mediator in the response to tunicamycin

Jan H. Reiling[a], Clary B. Clish[b], Jan E. Carette[a,1], Malini Varadarajan[a], Thijn R. Brummelkamp[a,2], and David M. Sabatini[a,b,c,d,3]

[a]Whitehead Institute for Biomedical Research, Cambridge, MA 02142; [b]Broad Institute of Massachusetts Institute of Technology and Harvard, Cambridge, MA 02142; [c]The David H. Koch Institute for Integrative Cancer Research, Massachusetts Institute of Technology, Cambridge, MA 02139; and [d]Howard Hughes Medical Institute, Department of Biology, Massachusetts Institute of Technology, Cambridge, MA 02139

This Feature Article is part of a series identified by the Editorial Board as reporting findings of exceptional significance.

Edited by Jonathan S. Weissman, University of California, San Francisco, CA, and approved May 16, 2011 (received for review December 6, 2010)

Tunicamycin (TM) inhibits eukaryotic asparagine-linked glycosylation, protein palmitoylation, ganglioside production, proteoglycan synthesis, 3-hydroxy-3-methylglutaryl coenzyme-A reductase activity, and cell wall biosynthesis in bacteria. Treatment of cells with TM elicits endoplasmic reticulum stress and activates the unfolded protein response. Although widely used in laboratory settings for many years, it is unknown how TM enters cells. Here, we identify in an unbiased genetic screen a transporter of the major facilitator superfamily, major facilitator domain containing 2A (MFSD2A), as a critical mediator of TM toxicity. Cells without MFSD2A are TM-resistant, whereas MFSD2A-overexpressing cells are hypersensitive. Hypersensitivity is associated with increased cellular TM uptake concomitant with an enhanced endoplasmic reticulum stress response. Furthermore, MFSD2A mutant analysis reveals an important function of the C terminus for correct intracellular localization and protein stability, and it identifies transmembrane helical amino acid residues essential for mediating TM sensitivity. Overall, our data uncover a critical role for MFSD2A by acting as a putative TM transporter at the plasma membrane.

gene trap | melibiose permease | KBM7 | dolichyl-phosphate (UDP-*N*-acetylglucosamine) acetylglucosaminephosphotransferase 1 (DPAGT1) | cancer

Tunicamycin (TM) has attracted much interest as an experimental tool to induce endoplasmic reticulum (ER) stress by inhibition of asparagine (N)-linked glycosylation, and its use has helped gain important insights into the intricate unfolded protein response (UPR) signaling network. TM is a mixture of related species of nucleotide sugar analogs fatty-acylated with alkyl chains of varying lengths and degrees of unsaturation (1) (Fig. 1*A*). It is naturally produced by several *Streptomyces* species and was originally described for its inhibitory role on the growth of viruses by impairing viral glycoprotein synthesis (2, 3). The TMs are inhibitors of a family of UDP-*N*-acetyl-D-hexosamine:polyprenol-phosphate *N*-acetylhexosamine-1-phosphate transferases (D-HexNAc-1-P-transferases) including the eukaryotic UDP-GlcNAc:dolichol phosphate GlcNAc-1-phosphate transferase (DPAGT1; also called GPT). TM has been proposed to either act noncompetitively as a substrate–product–transition state analog of DPAGT1/GPT (4) or a substrate analog inhibitor of D-HexNAc-1-P-transferases, suggesting that it competes with the UDP-HexNAc (UDP-GlcNAc in eukaryotes) for active site binding (5, 6).

Various environmental stimuli or changes in physiological conditions such as ER Ca^{2+} imbalance, hypoxia, alteration of ER redox state, glucose deprivation, or viral infection compromise the ER-luminal protein folding machinery and elicit a condition termed ER stress. When the folding capacity of the ER is overwhelmed by the increased client protein load that leads to accumulation of mis- and unfolded proteins in the ER lumen, a primarily cytoprotective signaling network is triggered known as the UPR. The UPR strives to regain ER homeostasis by multiple mechanisms including transient inhibition of protein synthesis, up-regulation of ER folding enzymes, and induction of ER-associated degradation (ERAD) (7). UPR induction leads to general inhibition of protein synthesis mainly mediated by the double-stranded RNA-dependent protein kinase (PKR)-like endoplasmic reticulum kinase (PERK). In addition, chaperones and ERAD machinery are up-regulated by two other major UPR branches involving activating transcription factor-6 (ATF6α/β) and the inositol-requiring enzyme-1 (IRE1α/β)/X-box binding protein-1 (XBP1) axis, which improves protein folding and reduces ER protein loading stress. IRE1 is a Ser/Thr kinase that contains an additional cytosolic endoribonuclease domain. On ER stress induction and IRE1 oligomerization/transphosphorylation, it splices *Xbp1* mRNA to generate a potent basic leucine zipper transcription factor whose targets include ERAD proteins and chaperones (8). PERK, ATF6, and IRE1 activation is regulated by the ER luminal chaperone glucose-regulated protein of 78 kDa (GRP78). If the stress imposed on the ER remains unresolved, prolonged activation of the UPR can lead to apoptosis (for instance, through the induction of the leucine zipper C/EBP homologous protein (CHOP) transcription factor downstream of the PERK/ATF4 axis) (7). ER stress and misregulated UPR signaling are associated with a variety of disease pathologies including diabetes, cancer, and neurodegeneration (9).

Besides its inhibitory action on DPAGT1/GPT, additional effects of TM include inhibition of protein palmitoylation (10) as well as ganglioside (11, 12) and proteoglycan biosynthesis (13) and reduction of 3-hydroxy-3-methylglutaryl coenzyme-A (HMG-CoA) reductase activity, the rate-limiting enzyme for the biosynthesis of cholesterol and isoprenoid derivatives (14, 15). The latter effect of TM might contribute to a block of *N*-glycosylation and cell proliferation by interfering with the assembly of the lipid glycosyl carrier dolichol (14). Prokaryotic members of the D-HexNAc-1-P-transferase family such as MraY, WecA, TagO, WbcO, WbpL, and RgpG are involved in the biosynthesis of dif-

Author contributions: J.H.R. designed research; J.H.R., C.B.C., J.E.C., M.V., and T.R.B. performed research; J.H.R., C.B.C., and D.M.S. analyzed data; and J.H.R. wrote the paper.

The authors declare no conflict of interest.

This article is a PNAS Direct Submission.

See Commentary on page 11731.

[1]Present address: Department of Microbiology and Immunology, Stanford University School of Medicine, Stanford, CA 94305.

[2]Present address: Netherlands Cancer Institute, Amsterdam, The Netherlands.

[3]To whom correspondence should be addressed. E-mail: sabatini@wi.mit.edu.

This article contains supporting information online at www.pnas.org/lookup/suppl/doi:10.1073/pnas.1018098108/-/DCSupplemental.

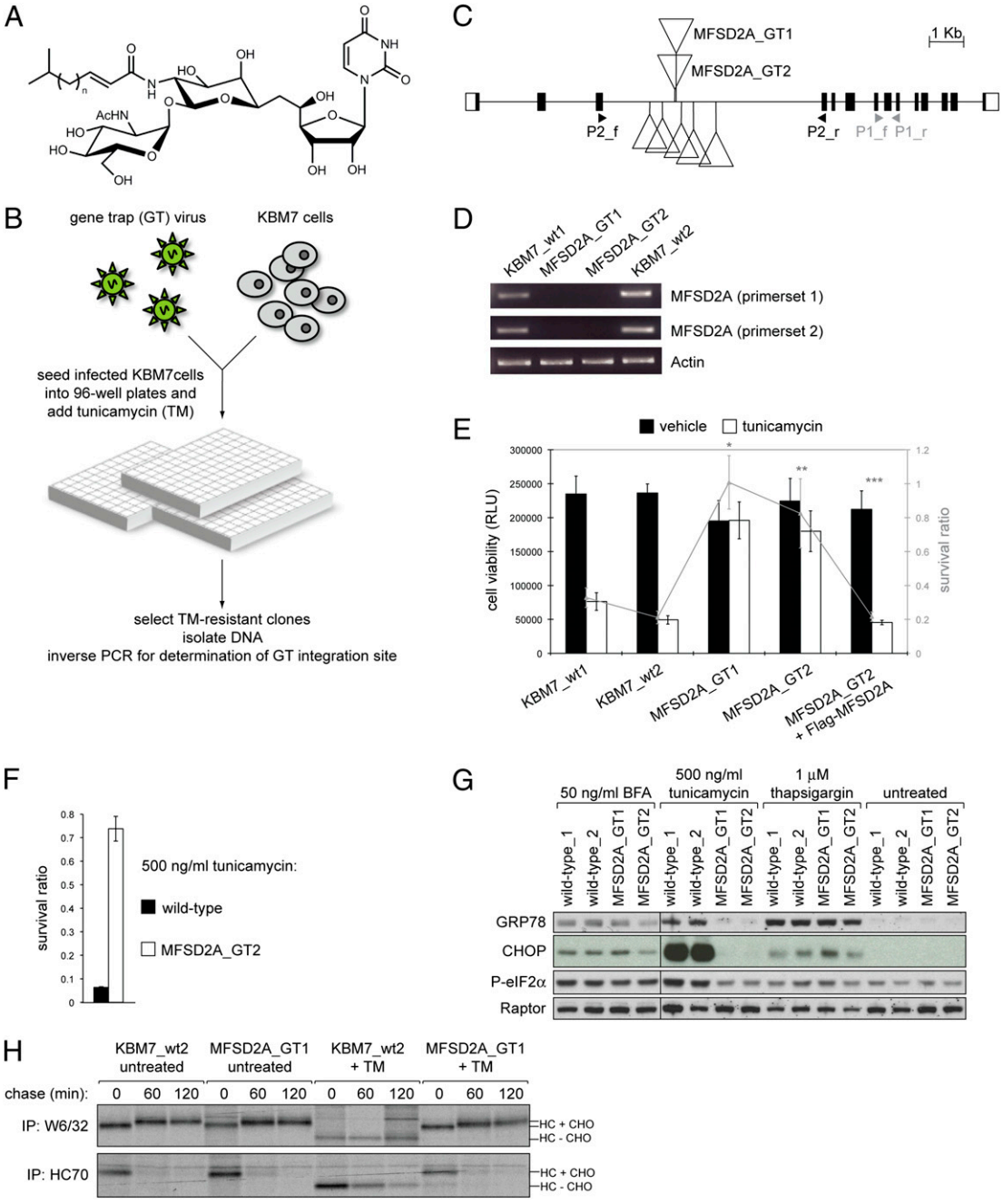

Fig. 1. Cells without MFSD2A are resistant to TM. (*A*) Structure of TM. TM is a mixture of homologous nucleotide sugar analogs differing in length (13–17 carbon atoms), branching, and unsaturation of their fatty acyl chain (n = 8–11). For simplicity, only one TM isomer type is shown. (*B*) Outline of the TM-resistance screen in the haploid KBM7 cell line. Details are given in the text. (*C*) Genomic locus of *MFSD2A* and GT insertions (triangles) found in the screen. White boxes denote the 5′ and 3′ untranslated regions, and black boxes denote coding exons. Arrowheads indicate primer binding sites of primersets 1 and 2 used for semiquantitative RT-PCR analysis (also in *D*). f, forward primer; r, reverse primer. (*D*) RT-PCR analysis of MFSD2A_GT1, MFSD2A_GT2, and WT KBM7 cells reveals no remaining *MFSD2A* mRNA in the GT lines using two different *MFSD2A* primer pairs. (*E*) MFSD2A GT1 (*$P < 3 \times 10^{-9}$) and MFSD2A GT2 (**$P < 2 \times 10^{-6}$) cells are significantly more resistant to TM compared with WT KBM7 cells (survival ratios of wt1 and wt2 were combined for Student two-tailed t test). Lentiviral introduction of a Flag-tagged *MFSD2A* cDNA construct into MFSD2A GT KBM7 cells restores the TM sensitivity phenotype comparable with that of WT cells (***$P < 1.4 \times 10^{-6}$; comparison between MFSD2A GT2 vs. MFSD2A GT2+Flag-MFSD2A). KBM7 cells were seeded into 96-well plates and grown for 40 h in the presence or absence of 500 ng/mL TM. Cell viability was determined using the CellTiter Glo (CTG) assay by comparing TM-treated with untreated wells (*Materials and Methods*). RLU, relative luminescence units. (*F*) MFSD2A_GT2 or WT KBM7 cells were grown in 96-well plates for 5 d in the presence or absence of 500 ng/mL TM, and cell survival was determined with the CTG assay. MFSD2A GT2 cells show a highly significant enhanced TM resistance ($P < 10^{-8}$). The survival ratio was calculated by dividing the mean values for treated cells by the untreated control values. Bars display survival ratio means ± SD of 11 wells for each condition. (*G*) Western blot analysis of two independent WT and MFSD2A GT KBM7 lines treated for 8 h with ER stress-inducing reagents before cell lysis. UPR signaling was assessed by immunoblotting with antibodies against different ER stress markers. The BFA-treated samples were run on a gel separate from the remaining lysates. (*H*) WT and MFSD2A GT1 KBM7 cells were labeled for 15 min with ^{35}S methionine, chased for the indicated time points in the presence or absence of TM, and lysed in 1% SDS before IP with indicated antibodies. HC + CHO, glycosylated class I MHC heavy chains; HC − CHO, deglycosylated class I MHC heavy chains.

ferent cell envelope polymers (16) and as such, offer prospects as potential antibacterial targets. There is also increasing interest in the development of new antifungal compounds to combat pathogenic fungi such as *Candida albicans*, and inhibition of N-linked glycolysation may be a promising approach (17).

N-glycosylation is a covalent posttranslational modification of proteins with the consensus Asn-X-Ser/Thr sequence (X ≠ Pro), and it is estimated that about 70–90% of all cellular proteins with this motif are cotranslationally *N*-glycosylated if they enter the secretory pathway (18). DPAGT1/GPT, which mediates the first committed step in the *N*-glycosylation pathway, is a multipass ER membrane protein that catalyzes the transfer of GlcNAc-1-phosphate from UDP-GlcNAc to the lipid carrier dolichol monophosphate (Dol-P) to form *N*-acetylglucosamine-pyrophosphatidyldolichol (GlcNAc-PP-Dol) (19). DPAGT1/GPT is the first enzyme in a series of 14 ER-associated glycosyltransferases assembling a 14-mer oligosaccharide core that is transferred en bloc onto asparagine residues within potential *N*-glycosylation sites by the oligosaccharyltransferase (OST) complex (19, 20).

N-glycan synthesis and branching are important features to help determine tumorigenic potential of cells (21, 22). TM displays significant cytotoxicity against transformed cells (23–26), and synergistic effects in combination treatments using TM and antineoplastic drugs [e.g., cisplatin, doxorubicin, vincristine, tumor necrosis factor-related apoptosis-inducing ligand (TRAIL), or erlotinib] have been reported (27–31). Nevertheless, the acute toxicity and small therapeutic window of TM have hampered its use for anticancer therapy so far. A better understanding of which host factors determine cellular TM sensitivity might therefore be helpful to assay for biomarkers and in the design of potential treatment regimens.

A wealth of studies using TM has been published since its discovery in the 1970s, but surprisingly, how TM enters cells has remained elusive. Here, we describe the identification and functional characterization of the major facilitator domain containing 2A (MFSD2A) transporter. We show that MFSD2A is a critical determinant of TM sensitivity: cells without MFSD2A are largely TM-resistant, whereas MFSD2A overexpression leads to increased cellular TM accumulation and massive TM susceptibility. In the latter case, C-terminal residues in MFSD2A are shown to be important for TM sensitization. Moreover, we identified two evolutionarily conserved amino acids in human MFSD2A, Asp-97 (D97) and Lys-436 (K436), that are important for establishing the TM hypersensitivity phenotype. Thus, MFSD2A is a candidate for the main plasma membrane TM transporter.

Results

Loss of MFSD2A Confers TM Resistance Upstream of GRP78 and DPAGT1/GPT. We used global gene disruption in a cell line haploid for all human chromosomes except for chromosome 8 to identify genes whose loss of function would render cells resistant to toxic doses of the N-linked glycosylation inhibitor TM (Fig. 1*B*). This insertional mutagenesis screening approach makes use of gene trap (GT) retroviruses that carry a strong splice acceptor site upstream of a promoterless and selectable marker gene. These haploid genetic screens have been recently used with success to identify cellular components required for influenza infection or toxicity to several bacterial toxins. GT insertions into genomic DNA of genes in KBM7 cells can lead to disruption of endogenous protein function and result in the generation of complete KOs (32).

KBM7 cells infected with GT retroviruses were grown in the presence of 500 ng/mL TM for ∼2 wk. Approximately 40×10^6 GT cells were screened. Several TM-resistant clones were obtained, and GT mapping revealed seven independent insertions in the *MFSD2A* locus (Fig. 1*C*). *MFSD2A* constitutes the sole bona fide hit in our TM resistance screen, because it was the only locus for which multiple independent GT insertions were recovered. MFSD2A has been previously identified in humans as a putative receptor for Syncytin-2, an ancient retrovirus-derived envelope protein that endows placental trophoblast cells with the capability to fuse into syncytiotrophoblasts (33). In mice, MFSD2A expression is induced during fasting periods in the liver and also during exposure to low temperatures in brown adipose tissue (34). In another study, tumor-suppressive functions were assigned to MFSD2A owing to its down-regulation in non-small cell lung cancer samples, decreased colony formation in vitro, and reduced tumor growth of MFSD2A-overexpressing A549 cells in mouse xenograft studies (35). A potential transporter function for MFSD2A has not been explored so far.

MFSD2A belongs to the large major facilitator superfamily (MFS) of transporters of which the lactose permease LacY of *Escherichia coli* is a well-studied example. Members of this family are found in all kingdoms of life, usually have 12–14 transmembrane segments, and transport a plethora of molecules including ions, sugars, nucleotides, amino acids, and drugs (36–38). Approximately 25% of all known membrane transporters in prokaryotes are represented by the MFS group (39). They are polytopic membrane proteins that serve as secondary carriers acting as uni-, anti-, or symporters. We used several secondary structure/hydrophathy programs and found that the algorithms mostly predicted 10 or 12 transmembrane domains for human MFSD2A with both the N and C termini oriented to the cytoplasm. In light of the homology of MFSD2A to other members of the glycoside-pentoside-hexuronide (GPH) family of MFS transporters (40), it is likely that MFSD2A contains 12 TM helices (e.g., http://minnou.cchmc.org/). A BLASTP search reveals the presence of MFSD2A homologs in vertebrates, but interestingly, no obvious ortholog is present in yeast, *Caenorhabditis elegans*, or *Drosophila*. A second MFSD2A-related protein (42% identity and 59% similarity in humans) with unknown function, MFSD2B, is present in higher eukaryotes as well (34). MFSD2A also shows homology to diverse bacterial sugar transporters including the melibiose permease (MelB), a cation/melibiose symporter (Fig. S1). Interestingly, TM is a natural product that includes a nucleotide sugar analog as a building block (1, 41).

Both MFSD2A GT cell lines used throughout this study have a similar cell size distribution as WT cells (Fig. S2*A*). Semiquantitative RT-PCR analysis of these two MFSD2A GT lines (henceforth named MFSD2A GT1 and GT2) revealed no remaining *MFSD2A* transcripts using two different primer pairs (Fig. 1*D*). Importantly, reconstitution of the MFSD2A_GT2 line with an epitope-tagged *MFSD2A* cDNA construct fully reverted the TM resistance phenotype to levels comparable with WT KBM7 cells (Fig. 1*E*). Thus, loss of MFSD2A causes cellular TM resistance. Viability of the MFSD2A GT cells after 5 d of treatment with 500 ng/mL TM was ∼70% compared with only 6% of WT cells (Fig. 1*F*). In agreement with these results, TM-treated WT KBM7 but not MFSD2A GT cells showed up-regulation of UPR markers such as the ER chaperone GRP78, the proapoptotic CHOP transcription factor, and phospho-eIF2α, a readout for general inhibition of translation (Fig. 1*G*). Notably, MFSD2A GT cells were as susceptible as WT cells to other ER stress-inducing drugs such as brefeldin A (BFA), thapsigargin, or DTT and showed similar UPR marker induction (Fig. 1*G* and Fig. S2*B*). Moreover, pulse-chase experiments with ^{35}S-labeled methionine showed that glycosylation and trafficking of newly synthesized class I MHC heavy chains using two different antibodies proceed unperturbed in the presence of TM in MFSD2A GT but not in WT KBM7 cells (Fig. 1*H*). This shows that, in cells without MFSD2A, the *N*-glycosylation pathway is not blocked despite the presence of TM in the culture media, suggesting that the compound does not reach its intracellular target DPAGT1/GPT at the ER. The slight decrease in survival of TM-treated MFSD2A GT cells is suggestive of parallel mechanisms or alternative routes of TM entry into cells that impact cell viability on exposure to high concentrations of this compound. For instance, TM may be able

to penetrate nonspecifically into the cell membrane by virtue of its lipophilic fatty acid moiety (41–43). Incomplete TM resistance may also be caused by other unknown proteins (for instance, MFSD2B) that act in a manner partially redundant to that of MFSD2A. Taken together, these results indicate that MFSD2A GT cells have no intrinsic ER stress-sensing defect and possess a functional UPR, and they suggest that TM-treated MFSD2A GT but not WT KBM7 cells maintain an unperturbed *N*-glycosylation pathway in the presence of the antibiotic. Therefore, TM resistance in *MFSD2A* mutant cells might be conferred upstream of known UPR components, presumably at the step of TM uptake into cells.

To establish where MFSD2A acts relative to the ER-luminal chaperone GRP78 and the TM target DPAGT1/GPT, which mediates the first step in the N-linked glycosylation pathway at the ER, shRNA-mediated double knockdown (KD) A549 cells were created (Figs. S2 *C* and *D* and S3 *C* and *E* show validation of hairpins; see Table S1 for shRNA sequences). The single GRP78 or DPAGT1 A549 KD cells are hypersensitive to TM and show a marked decrease in survival when exposed to different doses of TM, whereas MFSD2A-depleted cells display the opposite phenotype. Strikingly, simultaneous KD of MFSD2A/GRP78 or MFSD2A/DPAGT1 led to a TM-resistant phenotype very similar to the single MFSD2A KD phenotype (Fig. S3 *A* and *B*). Immunoblot analysis revealed a reduction of UPR marker expression in the shMFSD2A/shGRP78 or shMFSD2A/shDPAGT1 KD cells compared with control double KD cells (shLUC#221/shGRP78 or shLUC#221/shDPAGT1) or the single KD lines as expected (Fig. S3*C*). These findings were also recapitulated in KBM7 cells using four different DPAGT1 hairpins; single DPAGT1 KD KBM7 cells grown in TM-containing media quickly underwent apoptosis, whereas MFSD2A GT cells transduced with the same DPAGT1 hairpins were largely protected from cell death (Fig. S3*D*). In other words, to reveal TM hypersensitivity in cells with reduced GRP78 or DPAGT1 expression, MFSD2A function is required. The epistatic nature of the MFSD2A TM-resistant phenotype in the double KD cells is consistent with the hypothesis that MFSD2A might be involved in TM transport into cells upstream of GRP78 and DPAGT1/GPT.

To ask whether the function of MFSD2A in determining TM sensitivity is conserved across cells from different tissues, we infected several cancer cell lines with lentiviruses bearing shRNAs against MFSD2A for KD studies. Indeed, when using the most potent MFSD2A hairpin #1965, which leads to more than 70% or 80% reduction of *MFSD2A* mRNA levels in A549 and 786–0 cells, respectively (Fig. S2 *C* and *D*), significantly enhanced TM resistance was observed in A549, HT29, Jurkat T, HeLa, PC3, and 786–0 cells, which was evidenced by a greatly improved cell survival (Fig. S2 *E–J*). A similar, albeit weaker, TM resistance phenotype was noted when another MFSD2A hairpin (#1474) was used for KD studies; this finding is consistent with its less potent KD effect compared with #1965 in 786–0 cells (Fig. S2 *D* and *J*). Biochemical analysis of MFSD2A KD cells corroborated the finding that these cells experienced only little ER stress in response to TM as suggested by reduced GRP78 or CHOP expression (Fig. S2 *K* and *L*).

MFSD2A Is Glycosylated and Its Overexpression Sensitizes Cells to TM Treatment. Having established the widespread TM resistance phenotype upon loss of MFSD2A, we next investigated its gain of function effects. For this purpose, stable cell lines overexpressing MFSD2A or control proteins were generated. Using various lysis conditions, we were not able to detect tagged MFSD2A by immunoblotting from protein extracts of stable expressing cell lines. We therefore immunoprecipitated MFSD2A before Western analysis using antibodies against the epitope tag. The molecular weight of the cloned MFSD2A isoform predicted a protein of ~58.6 kDa; however, MFSD2A appeared as a smear of multiple bands, with the major band running around 70 kDa. TM treatment of Flag-MFSD2A–expressing cells before immunopurification (IP) or PNGase F digest of immunopurified MFSD2A led to a shift in band pattern compared with WT conditions, indicating that MFSD2A is a glycoprotein (Fig. 2 *A* and *B*). Interestingly, incubation of cells before IP with 10 ng/mL TM led to an identical band migration pattern as incubation with 1 μg/mL TM, suggesting that MFSD2A is already extensively deglycosylated at this low drug concentration (Fig. 2*A*). MFSD2A contains two predicted *N*-glycolysation sites (asparagines 217 and 227) in the extracelllular loop between transmembrane domains 5 and 6. We modified the WT *MFSD2A* cDNA by site-directed mutagenesis to abolish glycosylation of asparagines 217 and 227 (asparagine residues were converted into glutamine-encoding codons) in the protein (MFSD2AΔ*N*-glyco). Flag-MFSD2AΔ*N*-glyco immunopurified from stable A549 cells grown under normal conditions migrated similarly in a protein gel as Flag-MFSD2A treated with TM, and no additional band shift was apparent when Flag-MFSD2AΔ*N*-glyco cells were treated with TM before IP (Fig. 2*C*). This supports the notion that at least one, if not both, of the two MFSD2A asparagine residues in this context are normally glycosylated.

No obvious phenotypic alteration could be detected in cells overexpressing MFSD2A under normal culture conditions, with the exception of a slightly increased cell size in A549 cells (Fig. S4*A*), but these cells showed a proliferation rate indistinguishable from controls. An increase in the G1 and decrease in S phase of the cell cycle upon MFSD2A overexpression in A549 cells was recently reported (35). We next assessed the consequences of varying TM concentrations on A549 or PANC1 cells that stably overexpress MFSD2A. We observed a pronounced decrease in cell survival and a corresponding increase of UPR parameters in MFSD2A-overproducing cells using low TM concentrations that neither altered ER stress marker expression like GRP78, phospho-eIF2α, or CHOP in control cells nor affected their viability (Fig. 2 *D–F* and Fig. S4*B*). Overexpression of MFSD2AΔ*N*-glyco in conjunction with 50 ng/mL TM treatment led to a survival ratio comparable with WT MFSD2A expression, but the extent of apoptosis was somewhat reduced when a lower TM concentration (10 ng/mL) was used (Fig. S4*C*). The latter effect could be because of the decreased levels of the MFSD2A glycosylation mutant protein (Fig. 2*C*). Glycosylation of MFSD2A therefore is not a prerequisite for conferring TM sensitivity. A TM concentration as low as 1 ng/mL already had a strong effect on cell survival in MFSD2A-overexpressing A549 cells, whereas control cells showed no discernible effects at these concentrations (Fig. 2*E*). Additional control proteins containing transmembrane domains like MFSD2A such as Glut1, MFSD1, or lysosomal-associated membrane protein 1 (LAMP1), whose maturation involves processing through the secretory pathway, behaved indistinguishable from γ-Tubulin when overexpressed and treated with various TM doses (Fig. S4*D*), indicating that TM sensitivity in MFSD2A overexpressing cells is not caused nonspecifically through exhaustion of the endogenous UPR machinery (Fig. S4 *D* and *E*). Cell viability of γ-Tubulin– or Rap2a-expressing cells started to slightly decrease at TM concentrations ~40 ng/mL TM, and their survival ratio at 100 ng/mL TM was comparable with MFSD2A treated with 1 ng/mL TM (Fig. 2*E*). By monitoring dose-dependent effects of TM on UPR markers in MFSD2A-overproducing A549 cells, we found measurable increases in GRP78 protein levels at TM concentrations as low as 100 pg/mL (~120 pM) after 29 h of treatment. GRP78 levels were saturated at ~20 ng/mL TM, and no additional increases with even 50-fold higher TM doses were observed. CHOP expression was apparent with 10 ng/mL TM treatment, consistent with the strong decrease in cell survival. However, GRP78 levels in Flag-γ-Tubulin–expressing cells started to rise at ~40 ng/mL TM but did not reach a comparable GRP78 induction even with 1 μg/mL TM,

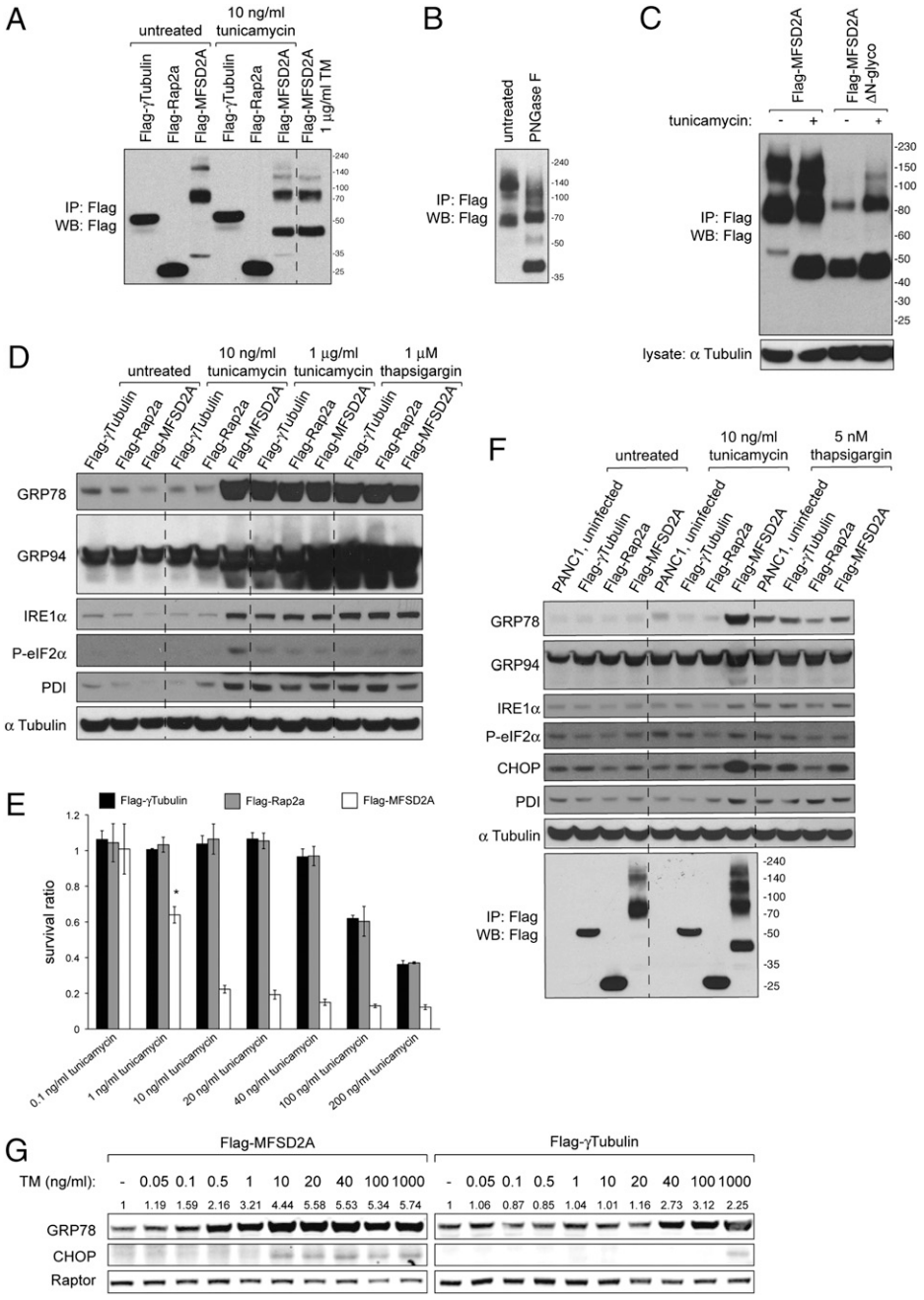

Fig. 2. MFSD2A glycosylation and effects of MFSD2A overexpression. (*A*) Stable A549 cells generated by lentivirus infection that overexpress the indicated proteins were grown for 24 h in the presence or absence of TM before cell lysis. The proteins were Flag affinity-purified, and immunoprecipitates were analyzed by SDS/PAGE followed by Western blotting. (*B*) Immunopurified MFSD2A was subjected to PNGase F digest and analyzed by SDS/PAGE and immunoblotting with anti-Flag antibody. (*C*) Stable Flag-MFSD2A– and Flag-MFSD2AΔN-glyco–expressing A549 cells were treated with 1 μg/mL TM for 24 h or left untreated. After cell lysis, Flag-purified MFSD2A or MFSD2AΔN-glcyo were subjected to Western blot analysis as described. (*D*) Stable A549 overexpressor lines mentioned in *A* were treated for 20 h with TM or thapsigargin. Lysates were analyzed by immunoblotting and probed with indicated antibodies. (*E*) The same overexpression lines described in *A* and *D* were subjected to chronic TM exposure. Flag-MFSD2A overexpressing cells are hypersensitive to TM [$*P < 0.001$ for 1 ng/mL TM and $P < 1.5 \times 10^{-6}$ (Student two-tailed *t* test) for the remaining higher TM concentrations; controls were pooled for statistical analysis]. Stable A549 cells were seeded into six-well plates (triplicate wells for each condition); 24 h after cell seeding, the culture media was replaced with fresh DMEM containing the indicated TM concentrations, and cell numbers were counted after additional 3 d ± TM with an automated Coulter Counter. Survival ratio was calculated from the number of surviving cells treated with TM divided by cell numbers of the untreated samples of the same genotype. (*F*) PANC1 cells stably expressing the indicated proteins were treated for 30 h with TM or thapsigargin, and lysates were analyzed by immunoblotting with antibodies shown. (*G*) TM dose-response analysis of stable A549 cells expressing Flag-MFSD2A (*Left*) or Flag-γ-Tubulin (*Right*; control) and treated with TM for 29 h. Values above GRP78 blots indicate the normalized GRP78 expression relative to Raptor levels. Blots were simultaneously processed and scanned using the Odyssey infrared imaging system (LI-COR). Quantitation of GRP78 expression was done by integrating pixel intensity of a defined rectangular area for each GRP78 protein band divided by the corresponding measurement for the Raptor control using Odyssey application software.

the highest TM concentration used (Fig. 2*G*). This indicates that A549 MFSD2A overexpressors are at least ~40- to 100-fold more sensitive to TM.

In accordance with the specific effects of TM on cells depleted of MFSD2A, no increased sensitivity to a variety of different ER stressors such as BFA, thaspigargin, DTT, and 2-DG as well as the topoisomerase II inhibitor etoposide was observed when MFSD2A was overexpressed (Fig. S4 *E* and *F*).

MFSD2A Mutants Reveal an Important Function of the C Terminus for Localization, Protein Stability, and Mediation of TM Sensitivity. To gain insight into subcellular localization of MFSD2A, we performed immunofluorescence (IF) staining and confocal microscopy on cells transiently transfected or stably expressing tagged MFSD2A. MFSD2A expression showed some variability between cells but presented as plasma membrane (PM) staining and cytoplasmic punctae (Fig. 3*A*). The punctae might represent MFSD2A-containing vesicles that shuttle between the endomembrane compartment and the PM. We obtained similar results using transiently transfected human embryonic kidney 293T (HEK293T) or stable EGFP-MFSD2A fusion protein-expressing HeLa and PANC1 cells (Fig. 3*A*). To confirm the specificity of the observed MFSD2A expression pattern, we repeated the experiment using Flag-tagged MFSD2A that was cotransfected with a GFP-Pleckstrin homology (GFP-PH) PM reporter into PANC1 cells (44). In agreement with the previous staining pattern, PM localization of Flag-MFSD2A was evident in addition to accumulation at some discrete cytoplasmic spots (Fig. S5*A*). Consistent with our results, Esnault et al. (33) recently showed cell membrane staining of HA-tagged MFSD2A expressed in HeLa cells. Mouse MFSD2A was reported to localize mainly to the ER, but PM staining was acknowledged as well (34).

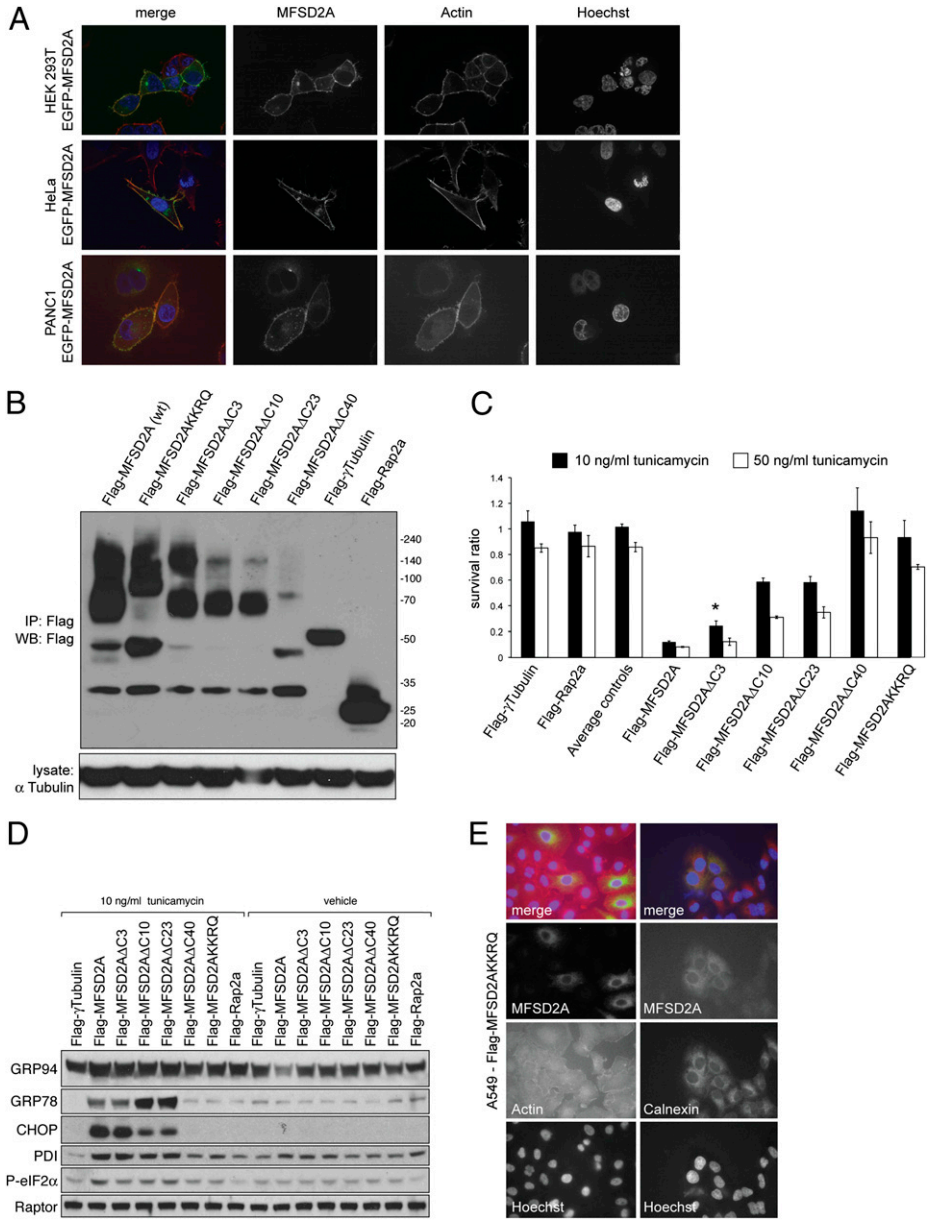

Fig. 3. MFSD2A localization and overexpression effects of MFSD2A mutants. (*A*) IF confocal microscopy of transiently transfected HEK293T (*Top*), stable HeLa (*Middle*), or stable PANC1 cells (*Lower*), all expressing EGFP-MFSD2A, reveals MFSD2A localization at the plasma membrane. Phalloidin and Hoechst were used to visualize the Actin cytoskeleton and nuclei, respectively. (*B*) SDS/PAGE followed by Western blot analysis of Flag-immunopurified MFSD2A mutants and control proteins from stable A549 cells. (*C*) Stable polyclonal A549 cell lines were established by lentiviral infection with MFSD2A C-terminal deletion mutants or the ER-targeted MFSD2A form (MFSD2AKKRQ; also in *E*) and tested for their ability to mediate TM sensitivity. All C-terminal MFSD2A mutant constructs shown are significantly less potent to induce apoptosis in conjunction with 10 ng/mL TM treatment than WT MFSD2A (*$P < 0.02$; P values for the remaining C-terminal mutants are all significant as well; i.e., $P < 0.01$). Cells were grown for 3 d in media with 10 or 50 ng/mL TM. Bars and error bars represent the mean ± SD of triplicate wells. (*D*) Immunoblot analysis of cell extracts from stable lines described in *B* and *C* treated for 30 h with TM or vehicle. (*E*) IF staining for Flag and Actin of A549 cells stably expressing Flag-MFSD2AKKRQ (*Left*). MFSD2A was visualized with an antibody against the Flag epitope. Costaining of MFSD2AKKRQ with the ER marker Calnexin shows overlapping staining patterns (*Right*).

C-terminal amino acid residues of xenobiotic transporters are important to ensure correct targeting, function, and expression at the PM by interaction with adaptor proteins. We scanned the amino acid sequence of MFSD2A and found that the last three C-terminal residues (Ser-Ile-Leu) fit a class I PDZ binding motif (45). To test the importance of the C terminus for MFSD2A function regarding TM sensitivity, a series of C-terminal MFSD2A deletion constructs (Flag-MFSD2AΔC) lacking the last 3, 10, 23, or 40 amino acids was engineered. Expression of these stable A549 MFSD2A deletion mutant cell lines was verified by IP followed by Western blot analysis. Removal of C-terminal amino acids caused electrophoretic mobility shifts likely attributable to the reduced molecular weight of the mutant proteins and changes in glycosylation pattern. Expression levels of the MFSD2AΔC forms generally seemed to be diminished compared with MFSD2A full-length protein (Fig. 3*B*). The importance of certain C-terminal amino acid residues for correct trafficking and expression of several transporters has been appreciated before (46–48).

To assess functionality of the MFSD2A deletion constructs, stable MFSD2AΔC lines were treated with two different doses of

TM for 3 d, after which time the surviving cells were counted. A549 cells that express WT MFSD2A showed the least numbers of viable cells at the end of the experiment (12% survival compared with 100% survival of control cell lines when treated with 10 ng/mL TM). Cells that expressed MFSD2A lacking the three C-terminal residues (MFSD2AΔC3) showed a significantly improved survival ratio (24% survival; $P < 0.03$ using Student two-tailed t test) compared with full-length MFSD2A. The viability ratio increased more in the MFSD2AΔC10 and MFSD2AΔC23 lines (59% and 58%, respectively). Notably, removal of the distal MFSD2A C-terminal 40 amino acids starting after the last transmembrane helix (MFSD2AΔC40) completely abrogated sensitivity to TM, and these cells showed the same viability as cell lines overexpressing control proteins without changes in GRP78 and CHOP levels (Fig. 3 *C* and *D*). IF staining of Flag-MFSD2AΔC40–expressing PANC1 cells showed that deletion of the last 40 amino acids prevented MFSD2A PM localization and instead, caused a reticular-like distribution that presumably reflects retention of the protein in the ER (Fig. S5*B*). Thus, we speculate that the C terminus of MFSD2A provides a binding platform for potential interaction partners required for correct MFSD2A trafficking and expression.

As mentioned earlier, TM interferes with glycoprotein biosynthesis by inhibiting the ER-localized glycosyltransferase DPAGT1/GPT. Its catalytic center has been proposed to act on the cytoplasmic side of the ER (49, 50). Cytoplasmic segments are also important for the catalytic activity of MraY, the bacterial homolog of DPAGT1/GPT (51). Thus, it is likely that, for TM to inhibit *N*-glycosylation, it does not need to permeate into the ER lumen. The TM resistance phenotype of cells without MFSD2A function could be explained by at least two possibilities. First, DPAGT1 levels might be increased in these cells. This seems unlikely, because quantitative real-time PCR for DPAGT1 in MFSD2A KD A549 and 786–0 KD cells did not show elevated *DPAGT1* mRNA levels (Fig. S6 *A* and *B*). Second, a failure of TM to reach ER-localized DPAGT1 (for instance, through prevention of TM uptake at the plasma membrane as suggested by the pulse-chase experiment (Fig. 1*H*) and the MFSD2AΔC40 mutant that is absent from the PM and unable to confer TM sensitivity) (Fig. S5*B*) should also cause TM resistance. Hence, we were interested in examining the consequences of mistargeting MFSD2A to the ER. Specific ER targeting was achieved by adding a dilysine motif to the C terminus of MFSD2A (MFSD2AKKRQ). Staining for the ER marker Calnexin and Flag-tagged MFSD2AKKRQ indeed showed MFSD2A/ER colocalization and very little MFSD2A staining at the cell membrane (Fig. 3*E*). Treating stable ER-targeted MFSD2A A549 cells with TM showed no increase in sensitivity, and their survival was indistinguishable from control cells using 10 ng/mL TM (Fig. 3*C*). A slight sensitization was observed using 50 ng/mL TM, probably caused by residual PM expression of a small MFSD2A pool that escaped ER retention. However, the small effect on survival was minor compared with WT MFSD2A overexpression. Thus, MFSD2A PM localization is crucial for conferring cellular TM sensitization.

To learn more about a possible mechanism for how TM sensitivity is mediated by MFSD2A and to explore its potential TM transporter function, we made use of two small molecules, Chlorpromazine (CPZ) and Phloretin, that both affect ion transport across the PM. CPZ inhibits various ATPases, including Na^+-K^+-ATPase, thereby reducing both the electrochemical sodium gradient and sodium-dependent solute transport (52, 53). Phloretin impinges on nonelectrolyte and ion membrane transport and more specifically, inhibits sugar, urea, and chloride transport (54). Interestingly, simultaneous treatment of MFSD2A-overexpressing cells with TM and CPZ or Phloretin largely negated GRP78 and CHOP induction observed with TM treatment alone (Fig. S7*A*). This raised the possibility that MFSD2A-mediated transport processes are ion-dependent (e.g., sodium-dependent).

MelB, a bacterial sugar symporter of the MFS with homology to MFSD2A, catalyzes the coupled symport of a cation (Na^+, Li^+, or H^+) with the energetically downhill movement of a galactoside such as melibiose, raffinose, or lactose (55). Through mutational analysis, several amino acids in MelB, including Arg-52 (R52), Asp-55 (D55), Asp-59 (D59), and Lys-377 (K377), have been identified that impair ion or sugar binding/translocation (56–62). The amino acid sequence alignment of MFSD2A and MelB shows that aforementioned residues are evolutionarily conserved (Fig. S1). We replaced selected amino acids of the WT sequence with alanines to create the corresponding MFSD2A mutants and asked whether these amino acid substitutions would alter MFSD2A activity regarding cellular TM susceptibility/transport. The following amino acids in MFSD2A were changed to alanine (A) residues: Arg-90 (R90A; corresponding to R52 in *E. coli* MelB), Asp-93 (D93A; D55 MelB), Asp-97 (D97A; D59 in MelB), and Lys-436 (K436A; K377 in MelB). A549 cells were transduced with the different MFSD2A mutant constructs by lentiviral infection and stable cell lines established before treatment with varying TM doses (ranging from 1 to 200 ng/mL TM) as described previously. We noted that, with the exception of the D93A and D97A mutants, all other MFSD2A mutant constructs showed reduced expression levels when Flag-immunopurified from stable A549-expressing cells, indicating that the amino acid substitutions render MFSD2A unstable (Fig. S7*B*). Of the MFSD2A constructs tested, only the D93A mutant showed similar survival ratios to the WT protein upon TM treatment, which is also reflected by their similar EC_{50} values [9.5 ± 0.02 and 14.1 ± 0.09 ng/mL TM for Flag-MFSD2A (WT) and Flag-MFSD2A(D93A), respectively]. However, overexpression of MFSD2A(D97A) displayed a dramatically weakened TM sensitivity phenotype, leading to an at least 9.4-fold EC_{50} shift [EC_{50} for Flag-MFSD2A (D97A): ≥89.5 ± 0.09 ng/mL TM] (Fig. S7*C*). Importantly, IF localization studies show that transfected Flag-MFSD2A(D97A) has an expression pattern indistinguishable from WT (Fig. S5 *A* and *C*). The findings suggest that D93 is largely dispensable for MFSD2A's ability to hypersensitize to TM, whereas D97 is critical. These results are in agreement with the behavior of previously described MelB mutants: Asp to Cys substitutions at positions 55 and 59 (D55C and D59C) in WT MelB have been shown to cause loss of sodium-coupled transport of melibiose; however, the D55C mutant (corresponding to D93A in MFSD2A) still retained H^+-coupled melibiose transport in contrast to D59C (D97A in MFSD2A), whose sugar transport activity is abolished because of elimination of cation (Na^+ and H^+) binding (56, 57, 59, 60). We surmise that the MFSD2A(D93A) mutant, which is equally potent in imparting TM sensitivity to cells as the WT protein, might still allow proton-coupled TM transport, whereas MFSD2A(D97A) does not.

The other two MFSD2A mutants tested in this assay, R90A and K436, displayed a similar dose-response curve as D97A or the negative controls (Flag-Glut1 and Flag-MFSD2AΔC40), but their reduced levels might have contributed to this phenotype (Fig. S7 *B* and *C*). For this reason, we transiently transfected HEK293T cells with the individual constructs to achieve comparable MFSD2A levels before treating the cells with TM. Both the transfected D97A and K436A mutants did not up-regulate the ER stress markers GRP78 and CHOP, whereas D93A and R90A did (Fig. S7*D*). Compared with WT Flag-MFSD2A, the K436A mutant displayed no appreciable PM localization but showed increased perinuclear staining suggestive of ER accumulation (Fig. S5*D*). Substitution of Ala, Ser, Gln, or Val for Arg-52 (R52) of MelB (R90 in MFSD2A) is critical for H^+-coupled melibiose transport but not essential for Na^+-coupled transport (61). Thus, by analogy, MFSD2A(R90A), despite its reduced expression levels in stably transduced A549 cells, might likewise still be able to couple sodium and TM cotransport,

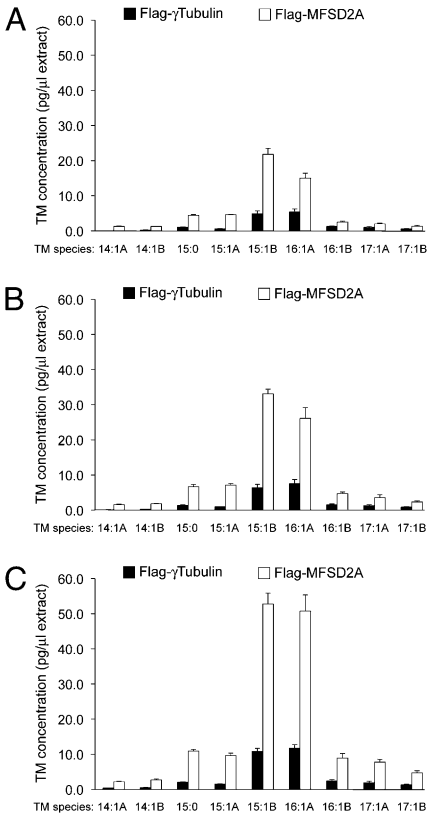

Fig. 4. Increased TM accumulation in cells overexpressing MFSD2A. 500 ng/mL TM treatment for 0.5 (*A*), 1 (*B*), or 3 h (*C*) shows a significantly enhanced and time-dependent TM accumulation in stable A549 Flag-MFSD2A overexpression cells compared with controls ($P < 0.03$ for all TM species and time points shown using Student two-tailed *t* test). A and B TM species nomenclature refers to geometric or positional isomers as suggested by Tsvetanova et al. (1). Total TM content of lysates was analyzed by MS (details in *Materials and Methods*). Values are the normalized mean concentration ± SD ($n = 3$).

which is inferred from its almost WT-like behavior in our HEK293T transfection assay (Fig. S7*D*). Last, a mutant MelB carrier, where Lys-377 (Lys-436 in MFSD2A) was substituted for Val (K377V), had significantly reduced sugar transport activity (62), and we find that the corresponding MFSD2A(K436A) mutant no longer evokes TM susceptibility and UPR marker induction upon overexpression, which is suggestive of impaired TM transport into cells (Fig. S7 *B* and *D*). Together, our IF stainings and gain of function results as well as the functional analysis of MFSD2A missense mutants hinted to a role for MFSD2A as PM TM transporter.

MFSD2A Overexpression Leads to Enhanced TM Accumulation in Cells. Based on (*i*) sequence similarity of MFSD2A to bacterial sugar permeases of the MFS, (*ii*) mutational analysis of conserved residues that have been shown to affect cation/sugar transport in MelB and likewise, critically influence MFSD2A's ability to induce ER stress upon TM treatment, (*iii*) its presence at the PM, (*iv*) normal Class I MHC heavy-chain trafficking and glycosylation in MFSD2A GT cells despite the presence of TM, (*v*) TM hypersensitivity of MFSD2A-overexpressing cells, and (*vi*) the fact that exclusive ER localization of MFSD2A or cytoplasmic accumulation of C-terminal MFSD2A deletion mutants did not elicit TM hypersensitivity, we surmised that TM might be a substrate for MFSD2A transported across the PM. We analyzed TM-treated MFSD2A KO KBM7 as well as stable A549 or PANC1 overexpressor cell lines for their TM content by MS. Because of its lipophilic fatty acid chain, TM is expected to nonspecifically partition into the lipid membrane bilayer independent of the genotype of the cells (43). Indeed, no differences in the intensity of the TM signal between the mutant and WT cells were detected (Fig. S8*A*). It is probable that the MS signal derived from nonspecific membrane binding of TM prevented us from detecting intracellular differences in TM accumulation, especially because intracellular TM accumulation might be much lower than the TM on the PM (43). In contrast, we readily detected significant differences in TM content in a time-dependent manner when cells were treated for different time periods with TM using the overexpression lines (Fig. 4 *A*–*C*). For instance, MFSD2A-overexpressing A549 cells displayed an approximately fivefold increase (depending on the TM species) after 3 h compared with cells overexpressing Flag-γ-Tubulin (Fig. 4*C*), but significant differences could already be detected after 30 min of TM treatment (Fig. 4*A*). In PANC1 cells, an ∼2- to 32-fold higher TM amount was measured in MFSD2A-overexpressing cells relative to controls after a longer exposure to the compound (Fig. S8*B*). Reassuringly, Flag-MFSD2AKKRQ A549 cells did not show elevated TM uptake (Fig. S8*C*) even after 24 h TM treatment. The ratios of the individual TM species accumulated in cells reflect the original TM stock composition used for this experiment, indicating that MFSD2A does not discriminate between the different TM homologs. For the same reasons alluded to earlier (i.e., the lipophilic nature of TM), the magnitude of the result might underestimate TM accumulation in MFSD2A-overexpression cells. In summary, WT but not ER-targeted MFSD2A expression causes increased cellular TM accumulation.

Discussion

Collectively, we have presented evidence for a major role of MFSD2A in determining cellular TM sensitivity. Its absence provides TM resistance, whereas overproduction has the opposite phenotype and is accompanied by increased TM uptake. MFSD2A is not the only determinant of TM sensitivity. TM's intracellular target, DPAGT1/GPT, is another critical component downstream of MFSD2A in the cellular response to TM. Increased DPAGT1/GPT expression can also confer TM resistance (63) (Fig. S9). Thus, the combination of both MFSD2A and DPAGT1/GPT levels will ultimately determine cellular TM sensitivity. At low doses, MFSD2A expression levels might be more critical, but at high TM concentrations, the antibiotic might passively enter cells; therefore, the levels of DPAGT1/GPT will be more vital. MFSD2A in conjunction with DPAGT1/GPT expression might serve as a biomarker for predicting cellular TM sensitivity.

It should be noted that some eukaryotes, including *C. elegans*, *Drosophila*, and yeast, do not possess obvious MFSD2A homologs but are still sensitive to TM treatment (64–66). Intracellular TM accumulation in these animals might be mediated by carriers unrelated to MFSD2A or passive diffusion of lipophilic TM. The latter effect can be readily appreciated, because even the MFSD2A KO (GT) cells described in this manuscript were not completely resistant to high TM doses, indicating that TM entered cells through partitioning and diffusion into the membrane lipid bilayer (Fig. 1*F* and Fig. S2*B*). TM concentrations commonly applied to yeast or *Drosophila* cells for UPR induction are usually orders of magnitudes higher than what we were using in some of our MFSD2A-overexpression experiments or even our haploid genetic screen for TM resistance (64–70). The TM effects observed in organisms without MFSD2A could be sufficiently explained by TM passively entering cells. It would be interesting to test and compare cell viability of yeast or *Drosophila* to mammalian cells at lower TM doses.

MFSD2A is a receptor for Syncytin-2 in the placenta that mediates cell fusion (33), but a potential transport function for MFSD2A has not been explored thus far. Interestingly, placental intrauterine growth restriction is correlated with significantly

decreased MFSD2A and glucose levels, raising the possibility that reduced MFSD2A function might lead to diminished accumulation of an unidentified growth-promoting substrate (71). Findings in mice that show MFSD2A up-regulation in liver and brown adipose tissue (BAT) upon fasting and cold-induced thermogenesis in BAT offer the possibility for a potential role of MFSD2A in uptake of an unknown molecule (34, 72).

Cotreatment/competition experiments of TM with several disaccharides, including the bacterial sugar melibiose, or a number of lipids have so far proven unsuccessful in identifying a potential physiological ligand for MFSD2A. Defined modifications to the structure of TM in conjunction with our overexpression cell system might help to pinpoint important structural features of TM for MFSD2A recognition. A more detailed understanding of the regulation of MFSD2A expression, trafficking, and interaction partners will aid elucidating a physiological function for this MFS transporter.

Materials and Methods

Cell Viability Assays. Viability of cells in 96-well assay plates with clear flat bottoms (Costar) was determined using the CellTiter Glo assay (Promega), which measures cellular ATP content. For suspension cells (KBM7 and Jurkat T cells), typically 20,000 cells were seeded per well. Culture volume per well was 100 μL. The cells were grown in the absence or presence of the drug for several days depending on the experiment; 50 μL CellTiter Glo reagent was added at the end of the experiment to lyse cells according to the manufacturer's protocol. ATP-based bioluminescence levels were measured using an EnVision plate reader (Perkin-Elmer). For low-throughput viability assays, 50,000–60,000 adherent cells were seeded in six-well clusters 24 h before drug addition. The next day, old media was aspirated and replaced with 2 mL fresh DMEM premixed with TM (or other drugs) before addition to the cells. Treatment duration usually was between 3 and 6 d depending on the cell line and experiment. For determination of cell number, cells were trypsinized and resuspended in media in a total volume of 3 mL. A 0.5-mL aliquot diluted 1:20 in Isoton II Diluent solution (Beckman Coulter) was used for cell number measurement using a Z2 Coulter Counter (Beckman Coulter). Cells with diameters between 10 and 30 μm were counted. Survival ratio was calculated by dividing cell numbers (or the luminescence signal) of the treated samples by cell numbers (or luminescence signal) of the untreated samples.

Western Blotting, Immunoprecipitations, and Pulse Labeling. Cells were harvested in lysis buffer containing 1% Nonidet P-40, 120 mM NaCl, 50 mM Tris·HCl (pH 7), 1 mM EDTA, 6 mM EGTA, 20 mM NaF, 1 mM benzamidine, 15 mM $Na_4P_2O_7 \times 10\ H_2O$ and freshly added complete Mini protease inhibitor mixture (Roche), 30 mM β-glycerophosphate, 30 mM para-nitrophenyl phosphate (pNPP), 4 μM Pepstatin, 400 μM PMSF, 2 μM aprotinin, and 4 μM leupeptin. Cell extracts were briefly vortexed and rotated for 10 min at 4 °C before centrifugation at 16.2 × *g* for an additional 10 min. For immunoprecipitations, a 50% slurry of anti-Flag M2 Affinity beads (Sigma) was washed three times in lysis buffer before IP. Between 500 μg and 1 mg protein and 40–50 μL slurry were used for IP by rotating samples for 2 h at 4 °C. Immunoprecipitates were washed three times with lysis buffer before elution, denaturation in 50 μL sample buffer, and boiling for 3 min. Bio-Rad protein assay was used to quantify protein amounts. Proteins were resolved on 4–12% NuPAGE Novex gradient Bis·Tris gels (Invitrogen) and transferred onto PVDF membranes (Immobilon). IgG-HRP–coupled secondary antibodies (Santa Cruz) for normal immunoblotting or fluorescently coupled IRDye 680 and 800 secondary antibodies (LI-COR Biosciences) for LI-COR analysis were used at 1:5,000 in 5% milk/PBS-T for 1 h incubation at room temperature. Proteins bands were visualized with Western Lightning chemiluminescence (ECL)/plus-ECL reagent (Perkin-Elmer) or LI-COR infrared scanner. Metabolic labeling and pulse-chase analysis were performed as described (73).

IF. HEK293T, A549, or PANC1 cells (60,000) were plated on coverslips (precoated with Fibronectin) in 12-well cluster plates; 24 h later, the cells were fixed for 15 min at room temperature in 4% paraformaldehyde solution (PFA) in PBS that was prewarmed to 37 °C, rinsed three times in PBS, and permeabilized for 5 min in 0.05% Triton-X in PBS. After an additional washing step with PBS, primary antibodies were diluted in 5% normal donkey serum, added to the cells, and incubated overnight at 4 °C. The slides were then rinsed three times with PBS and incubated for 1 h protected from light at room temperature with secondary antibodies (in 5% normal donkey serum) that were produced in donkey. After three more washes with PBS, the coverslips were mounted on glass slides using Vectashield (Vector Laboratories). Images were acquired either with a spinning disk confocal microscope (Perkin-Elmer) equipped with a Hamamatsu 1 × 1 k EM-CCD camera or a Zeiss Axiovert 200 M microscope equipped with a Zeiss AxioCam camera. Secondary Alexa Fluor antibodies were used at 1:2,000 dilution. Alexa Fluor 568 Phalloidin or Alexa Fluor 633 Phalloidin (Invitrogen) were used at 1:2,000, and Hoechst (Molecular Probes) was used at 1:2,000.

MS Analysis of Cellular Tunicamycin Content. Stable A549 cells (75,000) expressing the protein of interest were seeded 24 h before the addition of TM (Fig. 4). Cells were washed three times with ice-cold PBS before lysis in 250 μL 80% methanol. Samples were pipetted up and down several times, briefly vortexed, and stored at −80 °C before MS analysis. Measurement of TM was carried out using a 4000QTRAP triple quardupole mass spectrometer (AB SCIEX) that was coupled to an Agilent 1100 HPLC pump (Agilent Technologies) and an HTS PAL autosampler (Leap Technologies). Chromatographic separations were achieved using a 150 × 2.1 mm Atlantis T3 column (Waters) that was initially eluted isocratically at 250 μL/min with 50% mobile phase A (0.1% formic acid in aqueous 10 mM ammonium formate) and 50% mobile phase B (0.1% formic acid in acetonitrile) for 2 min followed by an 8-min linear gradient to 100% mobile phase B. Mass spectrometer settings used for multiple reaction monitoring (MRM) analyses of TM species were determined by infusion of a references solution. MRM transitions monitored using a 75-ms dwell time and collision energy setting of 25 were *m/z* 817.6/596.6 (Tun 14:1 A and B), 833.6/612.6 (Tun 15:0), 831.6/624.7 (Tun 15:1 A and B), 845.6/624.7 (Tun 16:1 A and B), and 859.7/638.7 (Tun 17:1 A and B). Other instrument settings were curtain gas = 20, electrospray source potential = 5 kV, source temperature = 400 °C, gas1 = 35, gas2 = 40, and declustering potential = 60. Calibration curves were generated by analysis of a serially diluted TM reference solution. Cell extracts were analyzed directly with 10 μL injected from each sample. MultiQuant software (version 1.1; AB SCIEX) was used for peak integration, and data were manually reviewed for quality of integration. TM signal intensities were normalized to cell number and averaged from three biological replicates.

ACKNOWLEDGMENTS. We thank Jason Moffat, Carson Thoreen, and Roberto Zoncu for reagents, Lan Guan for insightful discussions on MelB, Priya Kirubakaran for help with the TM structure illustration, Britta Mueller for assistance with the pulse-chase experiment, Hidde Ploegh for reagents, critical reading, and valuable comments on the manuscript, and the Broad RNAi platform for RNAi screening help. D.M.S. is an Investigator of the Howard Hughes Medical Institute. This work was supported by a Human Frontier Science Program (HFSP) fellowship (to J.H.R.) and National Institutes of Health Grants R21 HG004938-01 (to T.R.B.), CA103866 (to D.M.S), and CA129105 (to D.M.S).

1. Tsvetanova BC, Kiemle DJ, Price NP (2002) Biosynthesis of tunicamycin and metabolic origin of the 11-carbon dialdose sugar, tunicamine. *J Biol Chem* 277:35289–35296.
2. Takatsuki A, Tamura G (1971) Effect of tunicamycin on the synthesis of macromolecules in cultures of chick embryo fibroblasts infected with Newcastle disease virus. *J Antibiot (Tokyo)* 24:785–794.
3. Leavitt R, Schlesinger S, Kornfeld S (1977) Tunicamycin inhibits glycosylation and multiplication of Sindbis and vesicular stomatitis viruses. *J Virol* 21:375–385.
4. Heifetz A, Keenan RW, Elbein AD (1979) Mechanism of action of tunicamycin on the UDP-GlcNAc:dolichyl-phosphate Glc-NAc-1-phosphate transferase. *Biochemistry* 18:2186–2192.
5. Keller RK, Boon DY, Crum FC (1979) N-acetylglucosamine-1-phosphate transferase from hen oviduct: Solubilization, characterization, and inhibition by tunicamycin. *Biochemistry* 18:3946–3952.
6. Brandish PE, et al. (1996) Modes of action of tunicamycin, liposidomycin B, and mureidomycin A: Inhibition of phospho-N-acetylmuramyl-pentapeptide translocase from *Escherichia coli*. *Antimicrob Agents Chemother* 40:1640–1644.
7. Ron D, Walter P (2007) Signal integration in the endoplasmic reticulum unfolded protein response. *Nat Rev Mol Cell Biol* 8:519–529.
8. Hetz C, Glimcher LH (2009) Fine-tuning of the unfolded protein response: Assembling the IRE1alpha interactome. *Mol Cell* 35:551–561.
9. Kim I, Xu W, Reed JC (2008) Cell death and endoplasmic reticulum stress: Disease relevance and therapeutic opportunities. *Nat Rev Drug Discov* 7:1013–1030.
10. Patterson SI, Skene JH (1995) Inhibition of dynamic protein palmitoylation in intact cells with tunicamycin. *Methods Enzymol* 250:284–300.
11. Guarnaccia SP, Shaper JH, Schnaar RL (1983) Tunicamycin inhibits ganglioside biosynthesis in neuronal cells. *Proc Natl Acad Sci USA* 80:1551–1555.
12. Yusuf HK, Pohlentz G, Sandhoff K (1983) Tunicamycin inhibits ganglioside biosynthesis in rat liver Golgi apparatus by blocking sugar nucleotide transport across the membrane vesicles. *Proc Natl Acad Sci USA* 80:7075–7079.
13. Yanagishita M (1986) Tunicamycin inhibits proteoglycan synthesis in rat ovarian granulosa cells in culture. *Arch Biochem Biophys* 251:287–298.

14. Engström W, Larsson O (1988) The effects of glycosylation inhibitors on the proliferation of a spontaneously transformed cell line (3T6) in vitro. *J Cell Sci* 90: 447–455.
15. Volpe JJ, Goldberg RI (1983) Effect of tunicamycin on 3-hydroxy-3-methylglutaryl coenzyme A reductase in C-6 glial cells. *J Biol Chem* 258:9220–9226.
16. Price NP, Momany FA (2005) Modeling bacterial UDP-HexNAc: Polyprenol-P HexNAc-1-P transferases. *Glycobiology* 15:29R–42R.
17. Pierce CG, Thomas DP, López-Ribot JL (2009) Effect of tunicamycin on Candida albicans biofilm formation and maintenance. *J Antimicrob Chemother* 63:473–479.
18. Helenius A, Aebi M (2004) Roles of N-linked glycans in the endoplasmic reticulum. *Annu Rev Biochem* 73:1019–1049.
19. Bretthauer RK (2009) Structure, expression, and regulation of UDP-GlcNAc: Dolichol phosphate GlcNAc-1-phosphate transferase (DPAGT1). *Curr Drug Targets* 10: 477–482.
20. Jones J, Krag SS, Betenbaugh MJ (2005) Controlling N-linked glycan site occupancy. *Biochim Biophys Acta* 1726:121–137.
21. Lau KS, et al. (2007) Complex N-glycan number and degree of branching cooperate to regulate cell proliferation and differentiation. *Cell* 129:123–134.
22. Zhao YY, et al. (2008) Functional roles of N-glycans in cell signaling and cell adhesion in cancer. *Cancer Sci* 99:1304–1310.
23. Seiberg M, Duksin D (1983) Selective cytotoxicity of purified homologues of tunicamycin on transformed BALB/3T3 fibroblasts. *Cancer Res* 43:845–850.
24. Duksin D, Bornstein P (1977) Changes in surface properties of normal and transformed cells caused by tunicamycin, an inhibitor of protein glycosylation. *Proc Natl Acad Sci USA* 74:3433–3437.
25. Morin MJ, Bernacki RJ (1983) Biochemical effects and therapeutic potential of tunicamycin in murine L1210 leukemia. *Cancer Res* 43:1669–1674.
26. Carlberg M, et al. (1996) Short exposures to tunicamycin induce apoptosis in SV40-transformed but not in normal human fibroblasts. *Carcinogenesis* 17:2589–2596.
27. Jiang CC, et al. (2007) Tunicamycin sensitizes human melanoma cells to tumor necrosis factor-related apoptosis-inducing ligand-induced apoptosis by up-regulation of TRAIL-R2 via the unfolded protein response. *Cancer Res* 67:5880–5888.
28. Hiss DC, Gabriels GA, Folb PI (2007) Combination of tunicamycin with anticancer drugs synergistically enhances their toxicity in multidrug-resistant human ovarian cystadenocarcinoma cells. *Cancer Cell Int* 7:5.
29. Noda I, et al. (1999) Inhibition of N-linked glycosylation by tunicamycin enhances sensitivity to cisplatin in human head-and-neck carcinoma cells. *Int J Cancer* 80: 279–284.
30. Ling YH, Li T, Perez-Soler R, Haigentz M, Jr. (2009) Activation of ER stress and inhibition of EGFR N-glycosylation by tunicamycin enhances susceptibility of human non-small cell lung cancer cells to erlotinib. *Cancer Chemother Pharmacol* 64: 539–548.
31. Contessa JN, Bhojani MS, Freeze HH, Rehemtulla A, Lawrence TS (2008) Inhibition of N-linked glycosylation disrupts receptor tyrosine kinase signaling in tumor cells. *Cancer Res* 68:3803–3809.
32. Carette JE, et al. (2009) Haploid genetic screens in human cells identify host factors used by pathogens. *Science* 326:1231–1235.
33. Esnault C, et al. (2008) A placenta-specific receptor for the fusogenic, endogenous retrovirus-derived, human syncytin-2. *Proc Natl Acad Sci USA* 105:17532–17537.
34. Angers M, Uldry M, Kong D, Gimble JM, Jetten AM (2008) Mfsd2a encodes a novel major facilitator superfamily domain-containing protein highly induced in brown adipose tissue during fasting and adaptive thermogenesis. *Biochem J* 416:347–355.
35. Spinola M, et al. (2010) MFSD2A is a novel lung tumor suppressor gene modulating cell cycle and matrix attachment. *Mol Cancer* 9:62.
36. Pao SS, Paulsen IT, Saier MH, Jr. (1998) Major facilitator superfamily. *Microbiol Mol Biol Rev* 62:1–34.
37. Lewinson O, Adler J, Sigal N, Bibi E (2006) Promiscuity in multidrug recognition and transport: The bacterial MFS Mdr transporters. *Mol Microbiol* 61:277–284.
38. Saier MH, Jr., et al. (1999) The major facilitator superfamily. *J Mol Microbiol Biotechnol* 1:257–279.
39. Law CJ, Maloney PC, Wang DN (2008) Ins and outs of major facilitator superfamily antiporters. *Annu Rev Microbiol* 62:289–305.
40. Poolman B, et al. (1996) Cation and sugar selectivity determinants in a novel family of transport proteins. *Mol Microbiol* 19:911–922.
41. Duksin D, Mahoney WC (1982) Relationship of the structure and biological activity of the natural homologues of tunicamycin. *J Biol Chem* 257:3105–3109.
42. Kuo SC, Lampen O (1976) Tunicamycin inhibition of (3H) glucosamine incorporation into yeast glycoproteins: Binding of tunicamycin and interaction with phospholipids. *Arch Biochem Biophys* 172:574–581.
43. Takatsuki A, Tamura G (1972) Preferential incorporation of tunicamycin, an antiviral antibiotic containing glucosamine, into the cell membranes. *J Antibiot (Tokyo)* 25: 362–364.
44. Várnai P, Balla T (1998) Visualization of phosphoinositides that bind pleckstrin homology domains: Calcium- and agonist-induced dynamic changes and relationship to myo-[3H]inositol-labeled phosphoinositide pools. *J Cell Biol* 143:501–510.
45. Kato Y (2007) Xenobiotic transporter-adaptor network. *Drug Metab Pharmacokinet* 22:401–408.
46. Harris MJ, Kuwano M, Webb M, Board PG (2001) Identification of the apical membrane-targeting signal of the multidrug resistance-associated protein 2 (MRP2/MOAT). *J Biol Chem* 276:20876–20881.
47. Zaarour N, Demaretz S, Defontaine N, Mordasini D, Laghmani K (2009) A highly conserved motif at the COOH terminus dictates endoplasmic reticulum exit and cell surface expression of NKCC2. *J Biol Chem* 284:21752–21764.
48. Larsen MB, Fjorback AW, Wiborg O (2006) The C-terminus is critical for the functional expression of the human serotonin transporter. *Biochemistry* 45:1331–1337.
49. Kean EL (1991) Topographical orientation in microsomal vesicles of the N-acetylglucosaminyltransferases which catalyze the biosynthesis of N-acetylglucosaminylpyrophosphoryldolichol and N-acetylglucosaminyl-N-acetylglucosaminylpyrophosphoryldolichol. *J Biol Chem* 266:942–946.
50. Dan N, Middleton RB, Lehrman MA (1996) Hamster UDP-N-acetylglucosamine: dolichol-P N-acetylglucosamine-1-P transferase has multiple transmembrane spans and a critical cytosolic loop. *J Biol Chem* 271:30717–30724.
51. Al-Dabbagh B, et al. (2008) Active site mapping of MraY, a member of the polyprenyl-phosphate N-acetylhexosamine 1-phosphate transferase superfamily, catalyzing the first membrane step of peptidoglycan biosynthesis. *Biochemistry* 47: 8919–8928.
52. Van Dyke RW, Scharschmidt BF (1987) Effects of chlorpromazine on Na+-K+-ATPase pumping and solute transport in rat hepatocytes. *Am J Physiol* 253:G613–G621.
53. Bhattacharyya D, Sen PC (1999) The effect of binding of chlorpromazine and chloroquine to ion transporting ATPases. *Mol Cell Biochem* 198:179–185.
54. Andersen OS, Finkelstein A, Katz I, Cass A (1976) Effect of phloretin on the permeability of thin lipid membranes. *J Gen Physiol* 67:749–771.
55. Yousef MS, Guan L (2009) A 3D structure model of the melibiose permease of Escherichia coli represents a distinctive fold for Na+ symporters. *Proc Natl Acad Sci USA* 106:15291–15296.
56. Matsuzaki S, Weissborn AC, Tamai E, Tsuchiya T, Wilson TH (1999) Melibiose carrier of *Escherichia coli*: Use of cysteine mutagenesis to identify the amino acids on the hydrophilic face of transmembrane helix 2. *Biochim Biophys Acta* 1420:63–72.
57. Ding PZ, Wilson TH (2001) The effect of modifications of the charged residues in the transmembrane helices on the transport activity of the melibiose carrier of *Escherichia coli*. *Biochem Biophys Res Commun* 285:348–354.
58. Pourcher T, Deckert M, Bassilana M, Leblanc G (1991) Melibiose permease of *Escherichia coli*: Mutation of aspartic acid 55 in putative helix II abolishes activation of sugar binding by Na+ ions. *Biochem Biophys Res Commun* 178:1176–1181.
59. Zani ML, Pourcher T, Leblanc G (1993) Mutagenesis of acidic residues in putative membrane-spanning segments of the melibiose permease of *Escherichia coli*. II. Effect on cationic selectivity and coupling properties. *J Biol Chem* 268:3216–3221.
60. Pourcher T, Zani ML, Leblanc G (1993) Mutagenesis of acidic residues in putative membrane-spanning segments of the melibiose permease of *Escherichia coli*. I. Effect on Na(+)-dependent transport and binding properties. *J Biol Chem* 268: 3209–3215.
61. Franco PJ, Wilson TH (1999) Arg-52 in the melibiose carrier of *Escherichia coli* is important for cation-coupled sugar transport and participates in an intrahelical salt bridge. *J Bacteriol* 181:6377–6386.
62. Franco PJ, Jena AB, Wilson TH (2001) Physiological evidence for an interaction between helices II and XI in the melibiose carrier of *Escherichia coli*. *Biochim Biophys Acta* 1510:231–242.
63. Criscuolo BA, Krag SS (1982) Selection of tunicamycin-resistant Chinese hamster ovary cells with increased N-acetylglucosaminyltransferase activity. *J Cell Biol* 94: 586–591.
64. Plongthongkum N, Kullawong N, Panyim S, Tirasophon W (2007) Ire1 regulated XBP1 mRNA splicing is essential for the unfolded protein response (UPR) in *Drosophila melanogaster*. *Biochem Biophys Res Commun* 354:789–794.
65. Lee D, Singaravelu G, Park BJ, Ahnn J (2007) Differential requirement of unfolded protein response pathway for calreticulin expression in *Caenorhabditis elegans*. *J Mol Biol* 372:331–340.
66. Chen Y, et al. (2005) Identification of mitogen-activated protein kinase signaling pathways that confer resistance to endoplasmic reticulum stress in *Saccharomyces cerevisiae*. *Mol Cancer Res* 3:669–677.
67. Travers KJ, et al. (2000) Functional and genomic analyses reveal an essential coordination between the unfolded protein response and ER-associated degradation. *Cell* 101:249–258.
68. Uccelletti D, et al. (2008) APY-1, a novel *Caenorhabditis elegans* apyrase involved in unfolded protein response signalling and stress responses. *Mol Biol Cell* 19: 1337–1345.
69. Kondylis V, Tang Y, Fuchs F, Boutros M, Rabouille C (2011) Identification of ER proteins involved in the functional organisation of the early secretory pathway in *Drosophila* cells by a targeted RNAi screen. *PLoS One* 6:e17173.
70. Fei W, Wang H, Fu X, Bielby C, Yang H (2009) Conditions of endoplasmic reticulum stress stimulate lipid droplet formation in *Saccharomyces cerevisiae*. *Biochem J* 424:61–67.
71. Ruebner M, et al. (2010) Impaired cell fusion and differentiation in placentae from patients with intrauterine growth restriction correlate with reduced levels of HERV envelope genes. *J Mol Med* 88:1143–1156.
72. Wu Q, et al. (2006) Fatty acid transport protein 1 is required for nonshivering thermogenesis in brown adipose tissue. *Diabetes* 55:3229–3237.
73. Mueller B, Lilley BN, Ploegh HL (2006) SEL1L, the homologue of yeast Hrd3p, is involved in protein dislocation from the mammalian ER. *J Cell Biol* 175: 261–270.